Eur. Phys. J. D **25**, 41–55 (2003)
DOI: 10.1140/epjd/e2003-00218-2

THE EUROPEAN PHYSICAL JOURNAL D

Structures, stabilities and ordering in Ni-Al nanoalloy clusters

M.S. Bailey[a], N.T. Wilson, C. Roberts, and R.L. Johnston[b]

School of Chemical Sciences, University of Birmingham, Edgbaston Birmingham B15 2TT, UK

Received 21 August 2002 / Received in final form 17 January 2003
Published online 17 July 2003 –

Abstract. A detailed study is made of the structures and relative stabilities of nickel and aluminium clusters and nickel-aluminium "nanoalloy" clusters, with up to 55 atoms, modelled by the many-body Gupta potential. Random search and genetic algorithms are used to find the lowest energy isomers (both geometrical and permutational). For the pure Al and Ni clusters, the lowest energy structures are identical for most nuclearities but different structures are found for clusters with 15–18 atoms — the Al clusters having non-icosahedral structures. For these nuclearities, we investigate the effect of doping Al atoms into pure Ni clusters and *vice versa*, finding that the replacement of a single atom by a dopant atom is often sufficient to change the cluster geometry. The lowest energy isomers of nanoalloy clusters with the approximate composition "Ni_3Al" generally have structures based on icosahedral packing, though truncated octahedral (fcc packing) motifs are also observed. In agreement with previous studies, the atom ordering in the mixed Ni-Al clusters is found to depend on the maximization of the number of Ni–Al interactions, the minimization of the cluster surface energy, and atom size effects.

PACS. 36.40.Mr Spectroscopy and geometrical structure of clusters – 61.46.+w Nanoscale materials: clusters, nanoparticles, nanotubes, and nanocrystals – 61.66.Dk Alloys

1 Introduction

1.1 Nanoalloy clusters

Clusters are aggregates of between a few and many millions of atoms or molecules. They may consist of identical atoms, or molecules, or two or more different species and can be studied in a number of media, such as molecular beams, the vapour phase, in colloidal suspensions and isolated in inert matrices or on surfaces [1]. Interest in clusters arises, in part, because they constitute a new type of material which may have properties which are distinct from those of discrete molecules or bulk matter and also because their properties often vary significantly as a function of size [1–3].

The range of properties of metallic systems can be greatly extended by taking mixtures of elements to generate intermetallic compounds and alloys [4]. In many cases, there is an enhancement in specific properties upon alloying, due to synergistic effects and the rich diversity of compositions, structures and properties of metallic alloys, has led to widespread applications in electronics, engineering and catalysis. The desire to fabricate materials with well defined, controllable, properties and structures, on the nanometre scale, coupled with the flexibility afforded by intermetallic materials, has generated interest in bimetallic alloy clusters, or "nanoalloys" [5–7].

One of the major reasons for interest in nanoalloy particles is the fact that their chemical and physical properties may be tuned by varying the composition and atomic ordering, as well as the size of the clusters. Their surface structures, compositions and segregation properties [8] are of interest as they are important in determining chemical reactivity, and especially catalytic activity [9,10]. Nanoalloy clusters are also of interest as they may display structures and properties which are distinct from those of the pure elemental clusters. There are also examples of pairs of elements (such as Fe and Ag) which are immiscible in the bulk phase but which readily mix in finite clusters [11].

A number of theoretical studies, mainly using empirical many-body potentials [12], have been performed on intermetallic clusters [6,7,13–22]. Calculations based on semi-empirical molecular orbital methods and density functional theory (DFT) have also been applied to the study of small bimetallic clusters [23–25].

Ni-Al clusters have been the subject of several previous theoretical studies [7,15–19,24] and have become useful models for investigating those factors which are responsible for determining the atomic ordering or segregation in nanoalloy clusters. Ni-Al clusters are also of importance in heterogeneous catalysis — for example synergistic effects have been observed in the reductive dehalogenation of

[a] *Present address*: Department of Chemistry and Chemical Biology, Baker Laboratory, Cornell University, Ithaca, NY 14853-1301, USA.
[b] e-mail: roy@tc.bham.ac.uk

aliphatic and aromatic halides and polychlorinated arenes by sub-nanometre sized Ni-Al particles [26].

Here, we report the application of random search and genetic algorithms to determine the structures and atomic distributions in pure elemental nickel and aluminium clusters and in Ni-Al nanoalloy particles with up to 55 atoms, with all interactions modelled by the Gupta many-body potential [27]. We have considered: the effect of doping Al atoms into Ni clusters and *vice versa*; the distribution of binding energies of isomers of pure and mixed 16- and 19-atom clusters; and the structures, stabilities and atom ordering in clusters with the approximate composition "Ni_3Al".

1.2 Homotops

On going from pure metal clusters to bimetallic nanoalloys, there is an increase in complexity, due to the presence of two different types of atoms, which leads to the possibility of isomers based on the permutation of unlike atoms, as well as the regular geometrical isomers (with different skeletal structures). Jellinek has introduced the term "homotops" to describe A_aB_b alloy cluster isomers, with a fixed number of atoms ($N = a + b$) and composition (a/b ratio), which have the same geometrical arrangement of atoms, but differ in the way in which the A and B-type atoms are arranged [7,15–17].

As the number of homotops rises combinatorially with cluster size, global optimization (in terms of both geometrical isomers and homotops) is an extremely difficult task. Ignoring point group symmetry, a single geometrical isomer of an N-atom AB cluster will give rise to:

$$^{N}P_{A,B} = \frac{N!}{N_A!N_B!} = \frac{N!}{N_A!(N-N_A)!} \qquad (1)$$

homotops, where N is the total number of atoms, N_A is the number of atoms of type A and N_B is the number of atoms of type B [28]. For a 20-atom $A_{10}B_{10}$ cluster, for example, there are 184 756 homotops, though many may be symmetry-equivalent. The total number of homotops of any composition for a given structural isomer is 2^N, which for a 20 atom cluster is approximately 10^6. The importance of considering homotops when searching for global minima can be appreciated by considering the hierarchy of isomers of Cu_6Au_7, for which López *et al.* found the first 15 lowest lying isomers to be homotops of the same geometrical structure [14].

1.3 Genetic algorithms

Whether one is using empirical potentials or *ab initio* theory to describe the bonding in clusters, one of the principal objectives is to find, for a given cluster size, the arrangement of atoms (or ions or molecules) corresponding to the lowest potential energy — *i.e.* the global minimum (GM) on the potential energy hypersurface. However, as the number of minima rises quasi-exponentially with increasing cluster size, finding the GM becomes increasingly difficult [29]. In the discussion presented below, although it can never be guaranteed absolutely that the GM for a particular cluster size and composition has been found, we will label the lowest energy isomer (or homotop) as the GM, for convenience.

The genetic algorithm (GA) [30–32] is a search technique based on the principles of natural evolution. It employs operators that are analogues of the evolutionary processes of genetic crossover, mutation and natural selection to explore multi-dimensional parameter spaces. A GA can be applied to any problem where the variables to be optimised (genes) can be encoded to form a string (chromosome), each string representing a trial solution of the problem. The GA operators exchange information between the strings to evolve new solutions. The GA approach operates in an essentially parallel manner — different regions of parameter space are investigated simultaneously, with information concerning different regions of parameter space being passed between the individual strings by the crossover procedure. In this way, genetic information is disseminated throughout the population.

A review of previous applications of GAs to cluster optimization has been presented elsewhere [33].

2 Computational details

2.1 The Gupta potential

Since, for large clusters (of hundreds or thousands of atoms) *ab initio* calculations are still, at present, unfeasible, there has been much interest in developing empirical atomistic potentials for the simulation of such species. Empirical potentials, such as the Gupta potential [27], are derived by fitting experimental data to values calculated using a potential of an assumed functional form. The Gupta potential is written in terms of repulsive (V^{r}) pair and attractive many-body (V^{m}) terms, which are obtained by summing over all (N) atoms:

$$V_{\mathrm{clus}} = \sum_{i}^{N} \{V^{\mathrm{r}}(i) - V^{\mathrm{m}}(i)\} \qquad (2)$$

where:

$$V^{\mathrm{r}}(i) = \sum_{j}^{N}{}' A\,(a,b) \exp\left(-p\,(a,b)\left(\frac{r_{ij}}{r_0\,(a,b)} - 1\right)\right) \qquad (3)$$

and

$$V^{\mathrm{m}}(i) = \left[\sum_{j}^{N}{}' \zeta^2\,(a,b) \exp\left(-2q\,(a,b)\left(\frac{r_{ij}}{r_0\,(a,b)} - 1\right)\right)\right]^{\frac{1}{2}}. \qquad (4)$$

In equations (3) and (4), r_{ij} is the distance between atoms i and j in the cluster and A, r_0, ζ, p and q are fitted to experimental values of the cohesive energy, lattice

Table 1. Parameters defining the Gupta potential for Ni-Al clusters [27].

Parameter	Ni–Ni	Ni–Al	Al–Al
A / eV	0.0376	0.0563	0.1221
p	16.999	14.997	8.612
r_0 / Å	2.4911	2.5222	2.8637
ζ / eV	1.070	1.2349	1.316
q	1.189	1.2823	2.516

parameters and independent elastic constants for the reference crystal structure at 0 K. The primes indicate summation over all atoms j, except $j = i$.

For Ni_xAl_y alloy clusters, the parameters take different values for each of the different types (Ni–Ni, Ni–Al and Al–Al) of interaction. In the above equations, a and b are the atom labels for atoms i and j respectively. The homonuclear (Ni–Ni and Al–Al) parameters were derived by fitting to the pure metals and are taken to be unchanged in the alloys. The heteronuclear (Ni–Al) parameters were obtained by Cleri and Rosato [27], by fitting energetic and lattice dynamical properties of crystalline Ni_3Al. Our own calculations have confirmed that the Gupta potential does indeed predict the stability of the bulk Ni_3Al phase [34].

The Gupta potential parameters used in this study are listed in Table 1 [27]. Considering the structures of the bulk phases, the pure elements and the 3:1 alloys have face-centred cubic (fcc) packing of atoms: the bulk alloys Ni_3Al and $NiAl_3$ have cubic symmetry ($L1_2$). The 1:1 alloy NiAl, however has a body-centred cubic (bcc) structure, with the Ni and Al atoms adopting a CsCl-type (B2) arrangement [4].

In the Gupta potential, the parameters p and q can be thought of as a measure of the range of the repulsive and attractive interactions respectively: the larger their value the shorter the range. Thus p is larger for nickel than for aluminium as the respective atomic (metallic) radii are $r(\mathrm{Ni}) = 1.25$ Å and $r(\mathrm{Al}) = 1.43$ Å [35]. Hence, repulsion of core electrons between neighbouring atoms starts to play a significant role at larger distances for aluminium than for nickel. Also, the larger value of the A parameter means that the pair term is more repulsive for Al than Ni. Turning to the attractive part of the potential, nickel has a longer range parameter (smaller q) but a smaller hopping integral (ζ) than aluminium. The cohesive energy of bulk nickel (4.44 eV) is larger than that of aluminium, (3.39 eV) [35], because of the greater attractive Ni–Ni interactions at long range (due to the smaller q value) and the reduced short range repulsions.

It should be noted that no mention has been made of the fact that nickel is magnetic. The Gupta potential makes no attempt to consider magnetism explicitly but magnetism is incorporated into the fitted parameters implicitly, as the properties of the bulk material are affected by its electronic and magnetic characteristics. Furthermore, using this potential, Cleri and Rosato have correctly predicted the structural changes occurring in Ni_3Al upon introduction of chemical disorder [27].

2.2 Cluster binding energy

From the total cluster potential energy V_{clus}, the average binding energy for an N-atom cluster is defined as the positive quantity:

$$E_b = \frac{-V_{\mathrm{clus}}}{N} \tag{5}$$

and the second difference in binding energy may be calculated as:

$$\Delta_2 E_b\,(N) = 2E_b\,(N) - E_b\,(N+1) - E_b\,(N-1) \tag{6}$$

$\Delta_2 E_b(N)$ represents the relative stability of an N-atom cluster with respect to its neighbours (*i.e.* clusters with $N-1$ and $N+1$ atoms).

2.3 The random search algorithm

The random search algorithm (RSA) is the simplest method for finding minima on a potential energy surface. It involves performing a large number of searches from random starting points. Each starting structure (for an N-atom cluster) is generated by picking N sets of coordinates at random, subject to the following conditions [36]:

- the atoms lie within a sphere of radius $R_{\mathrm{clus}} = r_0 \times N^{\frac{1}{3}}$,
- no two atoms can be closer than $r_{\min} = 0.7 \times r_0$,
- the shortest distance between an atom and its neighbours cannot be greater than $r_{\max} = 1.3 \times r_0$,

where r_0 is the nearest neighbour distance.

The first condition means that the cluster volume scales (correctly) linearly with N and also that the starting geometries tend to be pseudo-spherical and relatively close packed. In the case of potentials for elements and alloys which are close packed in the solid state (such as Ni, Al and Ni_3Al), it is a reasonable assumption that the global cluster minima will also be densely packed. The second condition precludes starting geometries which are too compressed, and hence very high in energy, and the third condition prevents initial geometries in which one or more atoms are not connected to the remainder of the cluster.

The potential energy and the average binding energy are calculated for the initial, unrelaxed cluster and the cluster energy is then minimised by relaxing the cluster geometry, using the quasi-Newton NAG routine $E04KAF$ [37], which utilises analytical first derivatives of the potential. The average binding energy of the relaxed cluster, corresponding to a minimum on the potential energy surface, is then recorded.

The RSA was used to search for global minima for pure Ni and Al clusters, and for a number of Ni-Al nanoalloy clusters, with up to 20 atoms. In each case, 2 000 random searches were performed.

2.4 The genetic algorithm for cluster geometry optimization

As our cluster geometry optimization GA has been described in detail previously [33,38], only a brief description is presented here.

For a given cluster nuclearity (N), a number of clusters (increasing from 10 to 30 with increasing cluster size) are generated at random and then energy-minimized, to form the initial population (the "zeroth generation"), as for the random search described above. Each cluster is then assigned a fitness value, based on its total potential energy ($V_{\rm clus}$), such that low energy clusters (more negative $V_{\rm clus}$) have high fitness and high energy clusters (less negative $V_{\rm clus}$) have low fitness. In this work we have used an exponential function, with the fitness (F_i) of the ith member of the population (with $V_{\rm clus} = V_i$) given by:

$$F_i = \exp(-3\rho_i) \tag{7}$$

where the dimensionless quantity:

$$\rho_i = \frac{V_i - V_{\rm min}}{V_{\rm max} - V_{\rm min}} \tag{8}$$

and $V_{\rm max}$ and $V_{\rm min}$ are the $V_{\rm clus}$ values of the highest and lowest energy clusters in the current population.

The selection of parents for mating is accomplished using a variant of the roulette wheel method, whereby a cluster is picked at random and is accepted for mating if its fitness value (F_i) is greater than a randomly generated number between 0 and 1. If the candidate cluster is rejected for mating, then another is picked and the process is repeated. In this way, low energy clusters (with high fitness values) are more likely to be selected for mating and, therefore, to pass on their structural characteristics. Once a pair of parents have been selected for mating, they are subjected to the crossover operation.

Crossover is carried out using a modified version of the cut and splice crossover operator of Deaven and Ho [39], wherein random rotations (about two perpendicular axes) are performed on both parent clusters and then both clusters are cut horizontally — parallel to the xy plane — and complementary fragments are joined together. For heteroatomic clusters, such as nanoalloy clusters, the crossover procedure has been modified in order to preserve the correct number of atoms of each type in the cluster [40–42]. The number of matings was set to be 80% of the population size. Unless selected for mutation, each offspring cluster is subsequently locally minimized.

While the mating/crossover operation leads to a mixing of genetic material in the offspring, no new genetic material is introduced. In an attempt to maintain population diversity, a mutation operator is introduced. Within our GA, mutation is performed on the set of offspring, with each offspring cluster having the same probability (0.1) of being mutated. In this study, mutation was accomplished by moving one third of the atoms in the cluster to new, randomly generated positions. After mutation, clusters are locally minimized.

The set of "old" clusters (from the previous generation) and "new" clusters (offspring and mutants) are now ranked in order of potential energy and those with the lowest potential energies (most negative $V_{\rm clus}$ values) are selected to form the next generation, such that the population size is constant. This "elitist" selection process is the analogue of natural selection in biological evolution.

The whole process of mating, mutation and selection is repeated for around 100 generations. Because of the stochastic nature of the GA, for each nuclearity and composition, the GA program is run several times and the best (lowest energy) structure is recorded.

The GA, which has been shown to be significantly more efficient than the RSA for finding low energy structures for larger clusters and when there are two different types of atom present [33,38,40], was employed to find global minima for clusters with the approximate composition Ni_3Al, having 20–55 atoms.

3 Results and discussion

3.1 Pure nickel and aluminium clusters

The GM found for the pure Al clusters Al_2–Al_{20}, after 2000 random searches for each nuclearity, are shown in Figure 1. Below each Al_N structure is an indication of whether the same structure is found to be the GM for the pure Ni_N cluster. The structures adopted for the smaller Al and Ni clusters are similar to those found to be the GM for a number of other metals using Gupta and other empirical potentials — *e.g.* tetrahedral M_4, octahedral M_6, pentagonal bipyramidal M_7 [36,40]. For M_7–M_{12}, the structures correspond to fragments of the 13-atom centred icosahedral cluster, which is the GM for M_{13}, while the GM for M_{14} has an atom capping a triangular face of the icosahedron. DFT calculations by Ahlrichs and Elliott, also give these structures as GM for small Al clusters, though they are often distorted by the Jahn-Teller effect [43]. For M_{19} the GM is found to adopt the familiar double icosahedral (DI) geometry, while M_{20} has an additional atom capping the waist of the DI. These icosahedral-based structures are again commonly found for a number of metals using the Gupta potential and other atomistic potentials, with such structures being stabilized by the large number of metal–metal bonds [28,36, 40,41,44–47]. A distorted DI structure is predicted to be a metastable isomer for Al_{19} according to the DFT calculations of Ahlrichs and Elliott [43].

The structures obtained for Ni clusters in this size range are in good agreement with previous calculations using the Ni Gupta potential [18,48–51]. They are also in reasonable agreement with studies using related many-body potentials for Ni, such as the Sutton-Chen (S-C) potential [52,53] and the corrected effective medium (CEM) method [54,55], though there is significant disagreement with the tight binding calculations of Lathiotakis *et al.* [56]. The predicted GM for Ni_{19} and Ni_{20} are also in agreement with experimental studies, involving measuring the uptake of N_2 molecules by Ni, Ni-Fe and Ni-Al clusters, by Parks, Riley and coworkers [57–63].

Figure 1 shows that, for most nuclearities, the GM for the Al and Ni clusters are identical. A recent study of Ni-Al clusters (also using the Gupta potential), by Rexer *et al.* [18], has shown that for Ni-Al clusters with 12–14 atoms, the GM has the same geometrical structure for

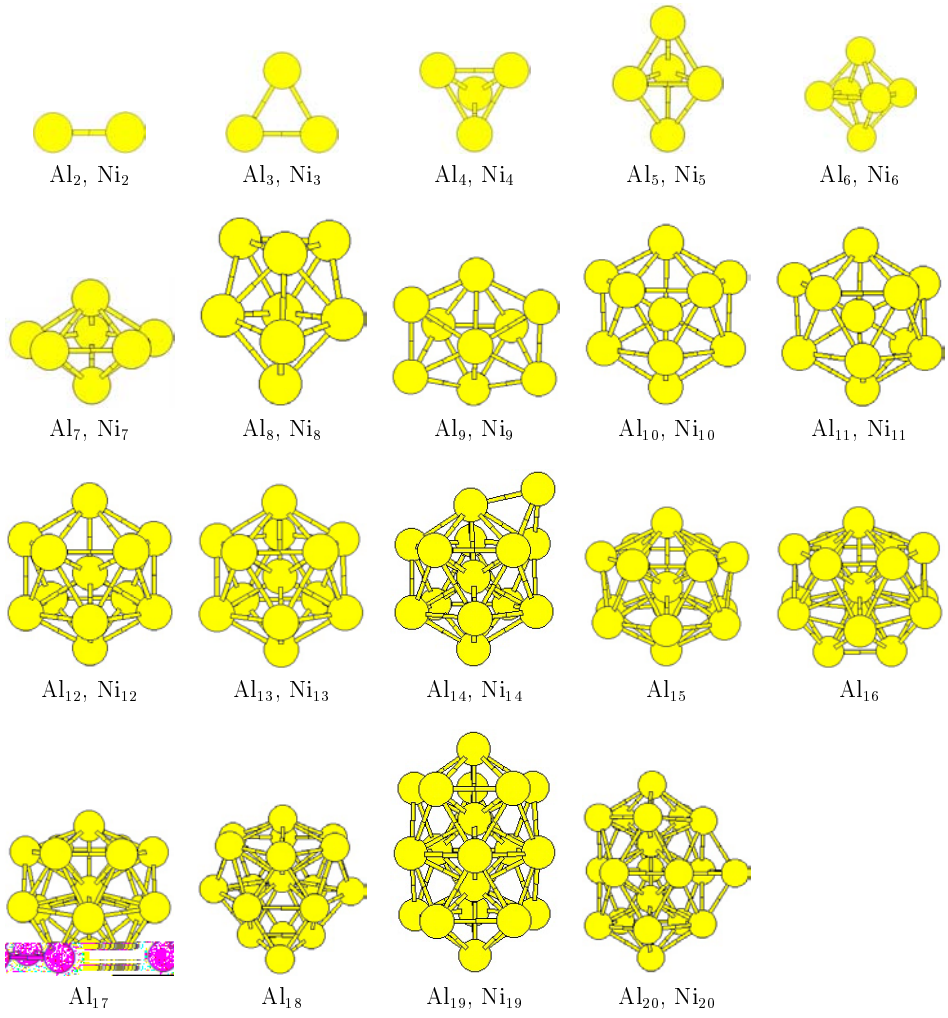

Fig. 1. GM found for the pure Al clusters Al_2–Al_{20} using the RSA. Beneath each structure it is also indicated whether the GM for the pure Ni cluster adopts the same geometry.

all compositions — from the pure Al to the pure Ni cluster — with the structures being as shown in Figure 1. We have found, however, that the structures of the GM for Al_N and Ni_N clusters are different for $N = 15$–18 atoms. As shown in Figure 1, the GM structures for Al_{15}–Al_{18} are not derived by capping a centred icosahedral core (the normal growth pattern leading from the icosahedron to the double icosahedron). Instead, the Al_{15} cluster has a centred, bicapped hexagonal antiprismatic structure and Al_{16}–Al_{18} have related structures, where one of the hexagonal faces of the hexagonal antiprism is capped by a 2-, 3- or 4-atom fragment. For the Gupta potential, the GM for Ni_{15}–Ni_{18} have structures based on capping the centred icosahedron, with the GM for Ni_{18} merely being the DI with one axial atom removed. These icosahedral-based structures are found to be higher lying (metastable) isomers for Al_{15}–Al_{18}. It should be noted, however, that the S-C and CEM potentials both predict that Ni_{15} should also adopt the Al_{15}-type structure [52,54], and they also predict GM based on decahedral cores for Ni_{18}. Doye and Wales have also found our Al_{15} structure to be the GM for 15-atom clusters, bound by long-ranged S-C many-body potentials [44] and long-ranged Morse pair potentials [64]. The Al_{16} and Al_{17} structures are also similar to those found for long-ranged Morse potentials [64]. The reason why we obtain these structures as the GM for Al_{15}–Al_{17} may be due to the long-ranged nature of the repulsive pair component of the Gupta Al potential. It should also be noted that the structures of Al_{15}–Al_{17} may also be described as Frank-Kasper polyhedra [65].

The binding energies (per atom), E_b, for the GM for M_2–M_{20} (M = Al, Ni) are plotted in Figure 2. For the larger clusters ($N > 11$), Ni_N clusters have higher binding energies than Al_N clusters, which is consistent with bulk nickel having a higher cohesive energy (4.44 eV) than aluminium (3.39 eV) [35]. Studies of larger clusters (with up to 561 atoms) have confirmed that $E_b(Ni_N) > E_b(Al_N)$, with the binding energy approaching the bulk cohesive energy as cluster size increases [66]. However, Figure 2 also shows that, for clusters with $N \leq 11$, the situation is reversed, with the Al clusters having higher binding energies. A possible explanation for this phenomenon lies in the fact that the longer ranged nature of the attractive many-body component of the potential energy for Ni (corresponding to the smaller value of q) does not dominate until the cluster reaches a critical size of 12.

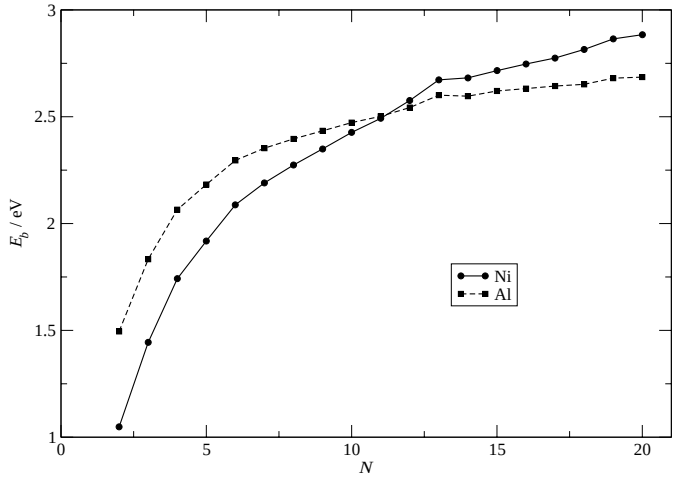

Fig. 2. Variation in binding energy (E_b) with cluster nuclearity for the GM of pure Ni and Al clusters.

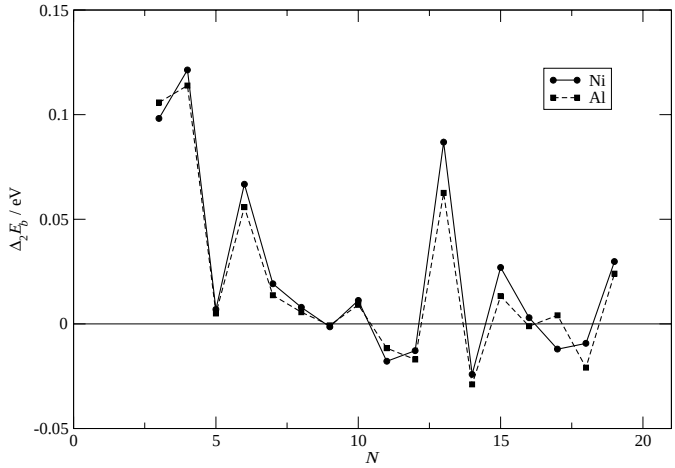

Fig. 3. The second difference in binding energy, $\Delta_2 E_b$, as a function of cluster nuclearity for the GM found for Al_3–Al_{19} and Ni_3–Ni_{19}.

Also, at around $N = 13$, atoms start to become encapsulated (*i.e.* bulk-like) so that the stabilising bulk-like cohesion may start to overcome the destabilization due to the surface at around this nuclearity. (It should be noted that the surface energies of comparable surfaces of nickel are considerably higher than those of aluminium [67,68].) However, the stabilization of small Al clusters, with respect to small Ni clusters is probably non-physical, since it is known that the Ni_2 dimer has a higher experimental binding energy per atom (1.04 eV) than Al_2 (0.80 eV) [24].

Figure 3 shows a plot of the second difference in binding energy, $\Delta_2 E_b$, as a function of cluster nuclearity for the GM found for Al_3–Al_{19} and Ni_3–Ni_{19}. The plots for Ni and Al clusters are almost identical throughout this region, with the exception of clusters with 15–18 atoms, where the GM (as discussed above) have different geometries for the two elements. Local maxima in the second difference plot correspond to structures which are stable with respect to "disproportionation" into larger and smaller clusters, with significant peaks found for high symmetry closed structures, such as the tetrahedron ($N = 4$), octahedron ($N = 6$) and icosahedron ($N = 13$). We would also expect there to be a maximum at $N = 19$, corresponding to the double icosahedron, for both Ni and Al. These structures maximize the average coordination number (and hence the binding energy) relative to their neighbours.

3.2 Nickel-aluminium nanoalloy clusters

3.2.1 Nickel doping of aluminium clusters

As mentioned above, the GM for Al and Ni clusters with 15–18 atoms were found to be structurally distinct, with the Al clusters having structures based on a centred hexagonal antiprismatic core, while the Ni clusters are based on a centred icosahedral core. This prompted an investigation into how many Al atoms in an Al_N cluster would have to be replaced by Ni atoms in order for the structure of the lowest energy isomer (the GM) of the nanoalloy cluster to conform to that of the Ni, rather than the Al cluster. The RSA was used in all cases.

Figure 4 shows that for Al_{15} and Al_{16} clusters, the replacement of a single Al atom by Ni is sufficient for the GM of the mixed cluster to adopt the (bicapped or tricapped icosahedral) structure of the pure Ni, rather than the pure Al cluster. (However, as will be discussed in the next Section, it is not always true that the same structure is adopted for all subsequent compositions up to the pure Ni_N cluster.) For Al_{17}, substitution of a single Al atom by Ni again results in a change of geometry and there is another change at Ni_2Al_{15}, yielding a structure corresponding to a DI with two atoms missing — however this is not the same geometry as the GM for Ni_{17} (which is a DI with three atoms missing and one atom capping the complete icosahedron) and this structure is only stabilized when there are four or more Ni atoms in the cluster. (The CEM calculations of Wetzel and DePristo found an alternative C_{2v}-symmetry structure for Ni_{17}[55], which is consistent with the experimental results of Parks and Riley [57,58].) For Al_{18}, the substitution of one to four Al atoms by Ni results in a DI with a non-axial atom missing. The Ni_{18} structure (a DI with a missing axial atom) is favoured for clusters with five or more Ni atoms.

Our results are in good agreement with previous studies on 13- and 14-atom Cu-Au clusters by López and coworkers [14] and by our calculations on 14-, 16- and 55-atom Cu-Au clusters [40], where it was found that the replacement of a single Au atom by Cu was sufficient to change the geometry of the GM from that of the pure Au to that of the pure Cu cluster. It should be noted, however, that for larger clusters, a small amount of doping is unlikely to result in a change in the GM structure, as the doping will then constitute a small perturbation to the cluster binding energy.

The inner atoms in icosahedral clusters of single elements tend to be under compression, so as to maximise surface atom interactions [45,69,70]. This leads to a destabilizing bulk strain energy [45]. As shown in Figure 4, in the four clusters studied here, the introduction of a single

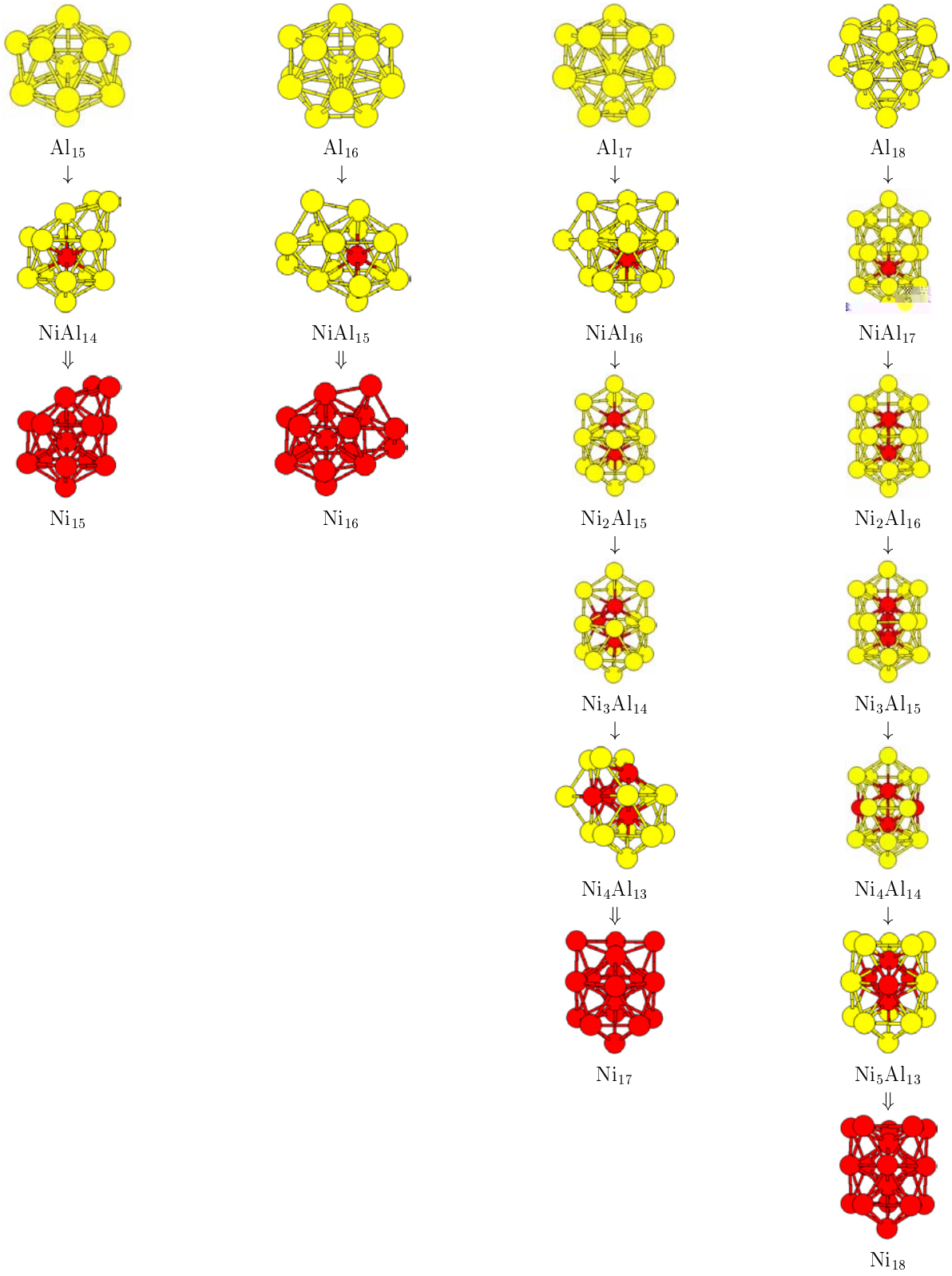

Fig. 4. Changes in geometric structure induced by doping Ni atoms into pure Al clusters for 15–18-atom clusters. The double arrows indicate that the nanoalloy cluster has the same geometry as the pure Ni cluster. It is not always the case, however, that the same structure is adopted for all intermediate compositions. (Al and Ni atoms are represented in yellow (light grey) and red (dark grey), respectively, here and in subsequent figures.)

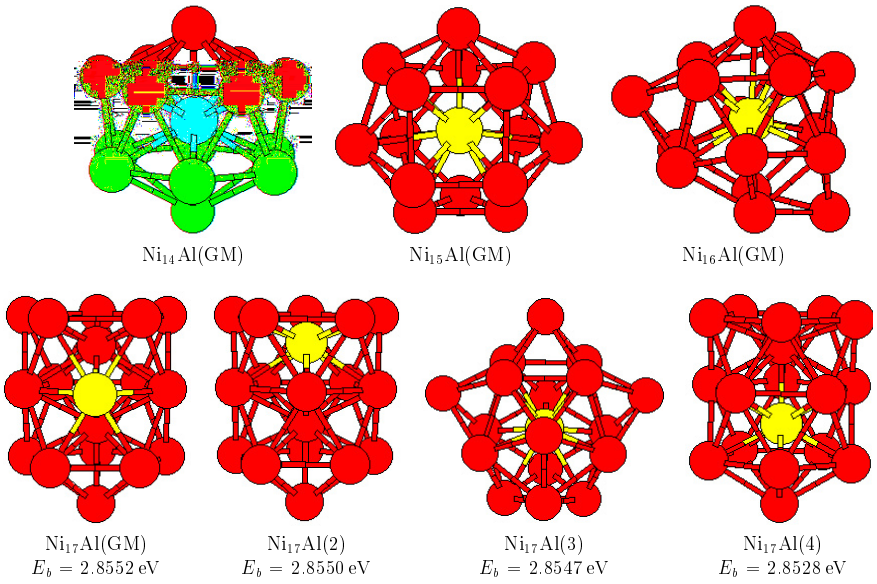

Fig. 5. GM found by the RSA for $Ni_{N-1}Al$ clusters, with N = 15–18 atoms. For $Ni_{17}Al$, the three lowest energy metastable isomers are also included, and the binding energies (E_b) are given.

Ni dopant atom stabilizes structures based on an icosahedral core, with the Ni atom located at the centre of the icosahedron. The location of the Ni atom in this central site is favoured by the smaller size of the Ni atom (r(Ni) = 1.25 Å), compared with Al (r(Al) = 1.43 Å) [35], which reduces the bulk strain energy. This also stabilizes such structures over the alternative, hexagonal antiprismatic structures found for the pure Al clusters. The preference for the smaller Ni atoms to adopt interstitial sites in mixed Ni-Al clusters has previously been discussed by Jellinek and Krissinel for icosahedral Ni-Al clusters with 13 atoms [15–17] and by Rexer *et al.* for 12–14-atom Ni-Al clusters [18].

Figure 4 also shows that for the 17- and 18-atom clusters, the second dopant atom goes preferentially into the centre of the second (incomplete) icosahedron, which is again consistent with the smaller atom going into the more sterically crowded site. The preference of Ni atoms for interstitial (bulk-like) sites is also favoured by the fact that elemental nickel has a significantly higher surface energy than aluminium (average surface energies are 149 meV Å^{-2} for Ni [67] and 71–75 meV Å^{-2} for Al [68]), so placing Ni atoms at the centre of the cluster lowers the surface energy of the cluster [19,22,71].

Jellinek has concluded that maximizing the Ni–Al mixing is the factor which determines the lowest energy structure when the composition, the geometry and the central atom type are specified [7,18]. For clusters with a small number of Ni atoms, occupation of the central site by Ni also serves to maximize the number of Ni–Al interactions. Inspection of Figure 4, for sequential doping into Al_{17} and Al_{18}, reveals that the third, fourth and fifth Ni atoms occupy sites which are in the waist of the incomplete double icosahedron. These sites have the greatest connectivity and, therefore the greatest number of Ni–Al interactions, although there must also be some Ni–Ni interactions. These findings are consistent with Jellinek's conclusions and can be explained in terms of the weaker repulsive pair interactions and stronger attractive many-body interaction in the Gupta potential for Ni–Al, as compared with Ni–Ni and Al–Al, which is a consequence of the fact that the ordered Ni_3Al phase has a higher bulk cohesive energy (4.57 eV [72]) than either bulk nickel (4.44 eV) or aluminium (3.39 eV) [35]. The Gupta potential is known to favour ordering in Ni_3Al, which also involves maximizing the number of Ni–Al interactions [27,34].

3.2.2 Aluminium doping of nickel clusters

Having studied Al-rich clusters, we now turn our attention to Ni-rich clusters with a single Al dopant atom. Figure 5 shows the GM (found by the RSA) for $Ni_{N-1}Al$ clusters, with N = 15–18. The structures of $Ni_{14}Al$, $Ni_{15}Al$ and $Ni_{16}Al$ are distinct from those of the pure Ni clusters. They also have interstitial Al, rather than Ni atoms, suggested that Ni–Al mixing is winning out over surface energy effects. The GM for $Ni_{14}Al$ is the bicapped centred hexagonal antiprism (the structure of the GM for Al_{15}) with the larger Al atom occupying the large cavity, thereby maximizing the number of Ni–Al interactions. The structure of the $Ni_{15}Al$ GM again has the Al atom in a large interstice, surrounded by 15 Ni atoms. These highly coordinated sites are therefore stabilized by having the larger Al atom surrounded by the smaller Ni atoms. For $Ni_{16}Al$, however, the central atom (again Al) is now in a slightly smaller interstice in a distorted capped pentagonal prismatic environment. This structure, which can also be viewed as a cross between decahedral and icosahedral coordination has previously been found as the GM for a number of 17-atom clusters — for example Ni_{17} and Au_{17} modelled by S-C potentials [44] and Pb_{17} modelled by a Gupta potential [75].

Figure 5 shows that, in the case of $Ni_{17}Al$, the GM has the same general structure (a DI with a missing axial vertex) as for Ni_{18}, as this structure has a greater average coordination number. The larger size of Al,

as compared with Ni, is manifested in the preference of the Al atom to occupy the highly-coordinated surface site (with 8 nearest neighbours), rather than an interstitial position, which would result in more Ni–Al interactions. Figure 5 also shows the three lowest lying metastable isomers for $Ni_{17}Al$, along with their calculated binding energies. The isomers $Ni_{17}Al$(GM), $Ni_{17}Al(2)$ and $Ni_{17}Al(4)$ are homotops, all having the axial-atom-deficient DI geometry and differing only in the position occupied by the dopant Al atom. It is interesting to note that the second and fourth lowest isomers have the Al atom in encapsulated positions, rather than occupying low-coordinated (with 5 or 6 nearest neighbours) sites. This implies that, for this nuclearity, the isomer stability order is the result of a fine balance between maximizing coordination number (and hence the number of Ni–Al interactions), minimizing the cluster surface energy, and minimizing bulk strain.

Finally, it should be noted that isomer $Ni_{17}Al(3)$ has an Al-centred capped pentagonal prismatic structure, which is related to the GM for $Ni_{16}Al$. The structure is slightly distorted away from a regular omnicapped pentagonal prismatic geometry so it does not possess a 5-fold symmetry axis. (Regular and distorted capped pentagonal prisms have been found in previous studies of metal clusters using empirical pair and many-body potentials [44,46].)

3.2.3 Comparison with experiment

In a detailed theoretical and experimental (N_2 uptake) study of Ni-Al clusters with 12–14 atoms, Rexer *et al.* have recently shown that the lowest energy structures for these nuclearities are based on the centred icosahedron, for all compositions [18] (with a surface atom removed or a capping atom added to give the 12- and 14-vertex clusters, respectively). This is consistent with our results, bearing in mind that we find the same icosahedral-based geometries for the pure Ni and Al clusters. The calculations reported by Rexer *et al.* for $Ni_{N-x}Al_x$ ($N = 12$–14), using the Gupta potential, indicate that the lowest energy homotops have Ni atoms at the centre of the icosahedron, for all compositions except $Ni_{N-1}Al$, but that there are low-lying metastable homotops, with interstitial Al atoms, which may also be detected by the N_2 uptake experiments [18].

In a recent experimental study of the uptake of N_2 by Ni_NAl clusters (with $N = 14$–19), Parks *et al.* found that the $Ni_{14}Al$ cluster initially saturates at $Ni_{14}Al(N_2)_{12}$ and finally (at higher pressures of N_2) saturates at $Ni_{14}Al(N_2)_{15}$, which is one fewer N_2 molecule than the maximum adsorbed by the pure Ni_{15} cluster [63]. These results have been interpreted in terms of a structure for $Ni_{14}Al$ which is the same as that for Ni_{15} — *i.e.* a bicapped icosahedron — with the Al atom substituting for one of the surface Ni atoms (though not one of the capping atoms). Our predicted GM for $Ni_{14}Al$, however, would be expected to saturate at $Ni_{14}Al(N_2)_{14}$ — with each of the 14 surface Ni atoms adsorbing one N_2 molecule. This may reflect an inadequacy in the Gupta potential (though it should be noted that a number of homotops with the bicapped icosahedral structure lie relatively close in energy to the GM, according to our calculations) or possibly an adsorption-induced reconstruction of the cluster [18].

The experimental results of Parks *et al.* for $Ni_{15}Al$ and $Ni_{16}Al$ also show adsorption of one fewer N_2 molecule than the pure Ni_{16} and Ni_{17} clusters, respectively [63]. For $Ni_{15}Al$ a tricapped icosahedral structure has been postulated (as for Ni_{16}), with a surface Al atom, thereby giving rise to a final saturation coverage of $Ni_{15}Al(N_2)_{15}$. In this case, the GM found for the Gupta potential, which has the Al atom in a larger interstitial site (see Fig. 5), should also saturate after the adsorption of 15 N_2 molecules, with each of the 15 surface Ni atoms adsorbing one molecule. Our GM for $Ni_{16}Al$, however, would be expected to adsorb up to 16, or even 18 N_2 molecules (as the 4-coordinate Ni atoms could possibly adsorb 2 molecules), in contrast to the observed saturation at $Ni_{16}Al(N_2)_{15}$ [63]. The observed saturation has been attributed to $Ni_{16}Al$ having the C_{2v} structure predicted by DePristo for Ni_{17} [55], with a central Ni atom and the Al atom on the surface of the cluster. Although our GM does not fit the experimental data, it is worth considering as a structure which may become accessible at higher temperatures.

In the case of $Ni_{17}Al$, Parks *et al.* found saturation at $Ni_{17}Al(N_2)_{15}$, which they attributed to a structure based on the lowest energy structure for Ni_{18} — a DI with one axial atom missing and with the Al atom replacing one of the Ni atoms in the middle M_5 ring [63]. This is the structure that we have identified as the GM for $Ni_{17}Al$ (see Fig. 5). The structures proposed for $Ni_{18}Al$ and $Ni_{19}Al$ are related to this structure by the addition of a Ni atom on the axis and capping the waist, giving the geometries that we have identified as the GM for Ni_{19} and Ni_{20}. Finally, it should be noted that the three lowest metastable isomers ($Ni_{17}Al(2)$–$Ni_{17}Al(4)$) shown in Figure 5, which have an interstitial Al atom, are not consistent with the experimental results of Parks *et al.*, since they would be expected to saturate at 17 N_2 molecules (or even higher for $Ni_{17}Al(3)$, which has three 4-coordinate Ni atoms) rather than the observed $Ni_{18}Al(N_2)_{16}$ [63].

3.2.4 Distribution of binding energies of 16-atom Ni-Al clusters

Figure 6 shows density of states histogram plots (*i.e.* distributions of distinct minima or isomers), as a function of binding energy, E_b, found after 2 000 random searches for the 16-atom clusters Al_{16}, Ni_{16} and Ni_8Al_8. The plot for Al_{16} is narrower and more sharply peaked than that for Ni_{16}, which may just be a consequence of the smaller Al–Al interaction terms in the Gupta potential giving rise to a smaller range of possible cluster binding energies. The average and maximum binding energies increase on going from Al_{16} to Ni_{16}, which is consistent with the greater strength of Ni–Ni binding [27].

The most striking feature of Figure 6 is the huge increase in the number of minima for Ni_8Al_8 (1702), as compared with the pure Ni_{16} (154 minima) and Al_{16} (202 minima) clusters. This is due to the very large number of

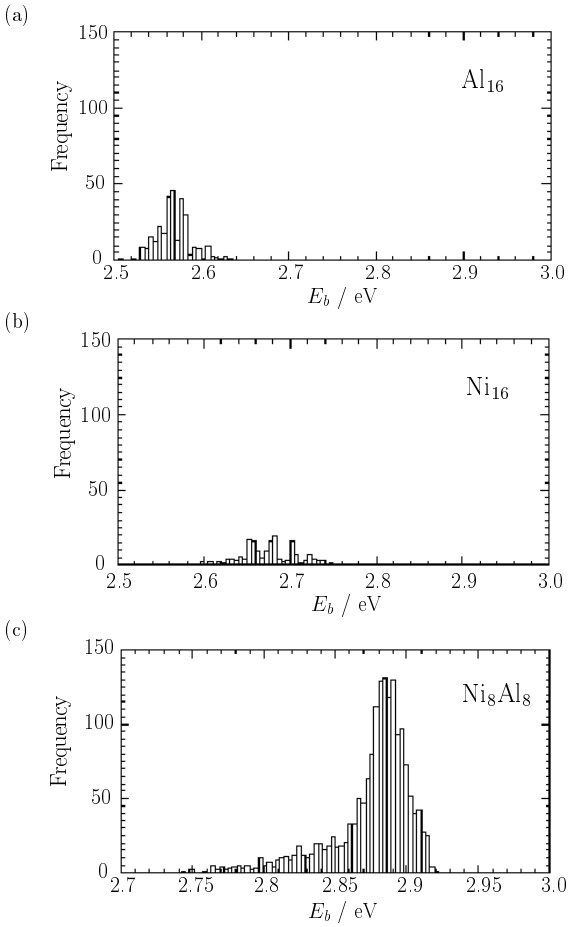

Fig. 6. Histograms representing the density of distinct isomers found (as a function of binding energy, E_b) from 2 000 random searches for the 16-atom clusters: (a) Al_{16}; (b) Ni_{16}; (c) Ni_8Al_8.

homotops possible for mixed Ni-Al clusters, which peaks at a Ni:Al ratio of 1:1. The mean, modal and maximum binding energies also increase, consistent with the greater strength of Ni–Al interactions, as compared to Ni–Ni and Al–Al interactions, which results in a negative enthalpy of mixing for Ni-Al alloys [72].

A similar analysis was carried out for 16-atom Ni-Al clusters with Ni:Al ratios of 3:1 ($Ni_{12}Al_4$) and 1:3 (Ni_4Al_{12}), for which 1 317 and 1 470 distinct minima were found, respectively. (These compositions have been chosen because they correspond to the stoichiometries of the fcc-type bulk Ni_3Al and $NiAl_3$ phases. Clusters with the approximate composition Ni_3Al will be discussed in more detail below.) The Ni-rich clusters were found to have higher mean, modal and maximum binding energies than the Al-rich clusters, due to the fact that Ni–Ni bonding interactions are greater than Al–Al interactions. Compared with Ni_8Al_8, however (see Fig. 6c), the 3:1 composition has lower average and maximum binding energies, because the Ni_8Al_8 cluster has more Ni–Al interactions and because the atomic environments in the 16-atom $Ni_{12}Al_4$ cluster are clearly very different from those in bulk Ni_3Al. The fact that the Ni–Al parameters were parameterised for solid Ni_3Al [27], which has a greater cohesive energy than any other pure or mixed Ni-Al phase [72], is reflected in the fact that the peak in E_b *vs.* composition is found to shift from a Ni:Al ratio of 1:1 towards 3:1 with increasing cluster size [66].

Table 2. Binding energies of GM isomers (E_b(GM)) found using the RSA for $Ni_{19-x}Al_x$ clusters. 2 000 random searches were performed for each composition.

Composition	E_b(GM) / eV
Ni_{19}	2.8643
$Ni_{18}Al$	2.9026
$Ni_{17}Al_2$	2.9381
$Ni_{16}Al_3$	2.9645
$Ni_{15}Al_4$	2.9897
$Ni_{14}Al_5$	3.0059
$Ni_{13}Al_6$	3.0209
$Ni_{12}Al_7$	3.0301
$Ni_{11}Al_8$	3.0340
$Ni_{10}Al_9$	3.0342
Ni_9Al_{10}	3.0309
Ni_8Al_{11}	3.0241
Ni_7Al_{12}	3.0101
Ni_6Al_{13}	2.9956
Ni_5Al_{14}	2.9734
Ni_4Al_{15}	2.9438
Ni_3Al_{16}	2.9074
Ni_2Al_{17}	2.8671
$NiAl_{18}$	2.7785
Al_{19}	2.6806

The distribution of minima shown in Figure 6c has a single large peak and a long tail at low E_b values. This is in contrast to the results obtained by Jellinek and Krissinel for 13-atom Ni-Al clusters [15–17]. Jellinek explored the populations of homotops for all compositions $Ni_{13-x}Al_x$ having the same, centred icosahedral geometrical structure. He found clear bimodal distributions, the populations of which were differentiated by the nature of the central atom: thus, (except for $Ni_{12}Al$) the more stable group were found to have Ni atoms in the centre and the least stable were Al-centred [15–17]. The fact that a bimodal distribution is not seen in Figure 6c is probably because our distribution includes geometrical isomers as well as homotops, so that any such effects are averaged out. The long tail at low E_b is due to particularly unfavourable combinations of geometric and permutational structures.

3.2.5 Structures and stabilities of 19-atom Ni-Al clusters

The binding energies, E_b(GM), of the GM found for $Ni_{19-x}Al_x$ clusters of all compositions, using the RSA (with 2 000 searches per composition), are listed in Table 2. The GM of $Ni_{10}Al_9$ has the highest binding energy.

One would expect the maximum number of Ni–Al interactions to be found for approximately this composition. The Ni-rich clusters have higher binding energies than the Al-rich clusters — *i.e.* the E_b(GM) values are greater for $Ni_{19-x}Al_x$ than for Ni_xAl_{19-x} for all x (with $x \leq 9$). For Ni_{19} and Al_{19}, this is consistent with the curves shown in Figure 2, and in all cases reflects the greater strength of Ni–Ni, as compared with Al–Al binding.

For mixed Ni-Al clusters, the number of distinct isomers tends to be greatest for approximately equal numbers of Ni and Al atoms, as these compositions give rise to greater numbers of homotops, by permutation of the Ni and Al atoms for each geometrical structural type. From 2 000 random searches for $Ni_{10}Al_9$ 1 709 distinct minima were found (excluding enantiomers, which have identical binding energies). Figure 7 shows 30 distinct isomers of $Ni_{10}Al_9$ (and their binding energies), which have been selected in 6 groups of 5 from the GM (with $E_b = 3.0342$ eV) to isomer number 1 709 (with $E_b = 2.8148$ eV). (*NB* as the RSA does not find all local minima, the minima shown here should be regarded as representative of those present in these energy bands.)

From Figure 7, it is apparent that the most stable isomers (those with highest binding energies) are homotops of the DI geometry. Variation from the DI structure does not appear until isomer 345. The lower lying DI homotops have two interstitial Ni atoms, while homotops with one interstitial Al atom are seen at intermediate energies (for example isomers 341, 343 and 344), though it is possible that such structures also occur earlier. We did not find any DI homotops with two interstitial Al atoms, probably because the larger Al atoms destabilise the structure and cause it to distort (placing two aluminium atoms in the centre of the DI structure would create a core too large to be satisfactorily covered by the remaining atoms whilst retaining the DI geometry).

The finding that the lowest energy homotops have internal Ni atoms is consistent with the findings of Jellinek and Krissinel (using the Gupta potential) for the icosahedral clusters $Ni_{13-x}Al_x$ [7,15–18]. As mentioned earlier however, the the Al-centred homotop was found to be slightly more stable (by less than 10^{-2} eV atom^{-1}) than the Ni-centred homotop for $Ni_{12}Al$. (This should be contrasted with $NiAl_{12}$, for which the Ni-centred homotop is favoured by approximately 0.1 eV atom^{-1} [15–17].) Embedded Atom Method (EAM) calculations by Rey *et al.*, however, predicted that the Ni-centred homotops are more stable than Al-centred homotops for all 13-atom icosahedral Ni-Al clusters [19]. This prediction is supported by DFT calculations, which reveal the Ni-centred homotop to be more stable than the Al-centred one by 0.04 eV atom^{-1} [24]. Rey *et al.* also predicted that, for $Ni_{19-x}Al_x$ clusters, with the DI geometric structure, the most stable homotops have two internal Ni atoms right up to $NiAl_{18}$ [19], which is consistent with our finding for $Ni_{10}Al_9$.

The GM for $Ni_{10}Al_9$, that we have obtained using the Gupta potential, has two Al atoms in the two axial (5-fold axis) sites, but among the five lowest energy homotops (with binding energies ranging from 3.0342–3.0319 eV) three have one Al and one Ni atom in the axial sites and two have two Al atoms. Homotops with two axial Ni atoms are less stable. The slight preference for axial Al atoms may be because these low-coordinate sites can better accommodate the larger Al atoms. It should be noted, however, that with the EAM potential employed by Rey *et al.*, the GM is predicted to have two axial Ni atoms [19] — so the result may be potential-dependent.

As the isomer stability decreases (*i.e.* for lower binding energies), the occurrence of the DI geometry becomes less frequent and less compact, often less symmetrical structures start to appear. This culminates with isomer 1 709 which is a structure composed of only two layers of atoms. The binding energy of this isomer (2.8148 eV) is considerably lower than isomer 1 708 (E_b = 2.8561 eV). Because our random generation process starts from pseudo-spherical distributions of atoms, very unstable linear and planar structures are discriminated against, though they may be local minima on the potential energy surface.

Finally, it is worth noting that isomer 854 is a DI homotop, but one with a relatively low binding energy (2.9612 eV), because it has one interstitial Al atom and the Ni and Al atoms tend to be grouped together — so that the number of Ni–Al contacts is small. Isomer 1534, on the other hand, is destabilised (E_b = 2.9325 eV) because one of the 8-coordinate waist atoms of the DI has been removed and now lies in a low-coordinate capping site on the other side of the cluster.

3.2.6 Using the genetic algorithm to find global minima for "Ni_3Al" nanoalloy clusters with 20–55 atoms

Ni_3Al is one of the most widely studied alloy phases [4]. It has the highest cohesive energy in the Ni-Al phase diagram [72] and it is likely that the Gupta model, which is based on the second moment approximation to tight binding theory [27], is more applicable for Ni-rich, rather than Al-rich phases. For these reasons, we decided to study the geometries, stabilities and atomic ordering properties of Ni-Al clusters with the approximate composition $Ni_{3x}Al_x$, having 20–55 atoms.

In previous studies of model and elemental clusters [33, 38, 47], we have shown that the GA is much more efficient than the RSA at finding global minima (*i.e.* the most stable geometrical isomer for a given nuclearity), especially for higher nuclearities. Recently, we have demonstrated that the GA is also efficient at finding the lowest energy homotops for a given nuclearity, composition and geometry for Cu-Au nanoalloy clusters [40]. We therefore decided to use the GA to search for GM for these larger nanoalloy clusters. The greater reliability of the GA for finding low-energy structures is demonstrated by the lowest energy structures found for the 20-atom $Ni_{15}Al_5$ cluster using the GA and RSA (2 000 random searches) methods. These structures are homotops, both having a waist-capped DI geometry but differing in the distribution of the Ni and Al atoms. The GA finds a lower energy homotop (E_b = 3.026 eV) than the RSA (E_b = 3.022 eV). In light of this

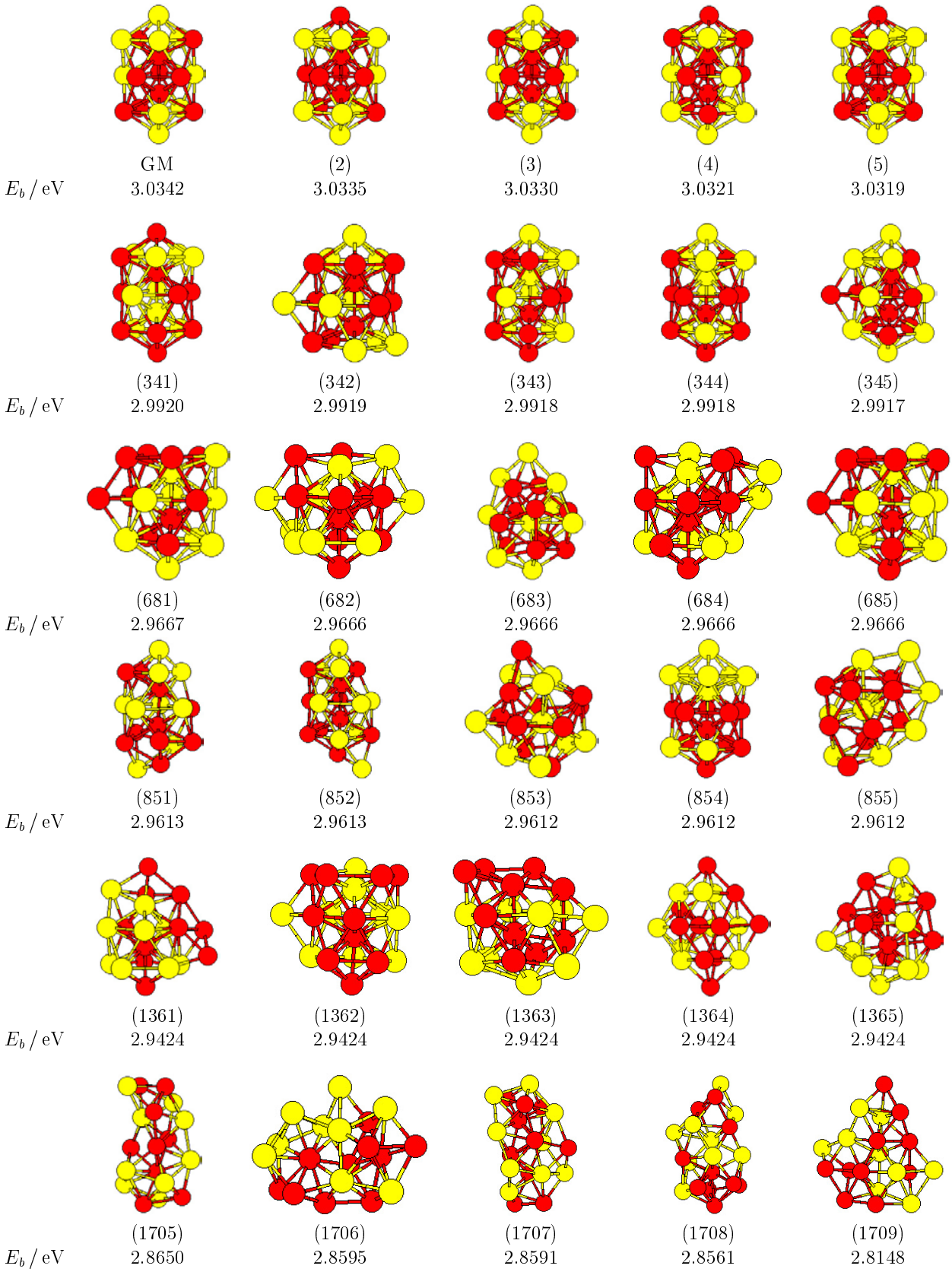

Fig. 7. 30 of the 1 709 distinct isomers of $Ni_{10}Al_9$ found by the RSA (from 2 000 searches). The binding energies (E_b) are also given.

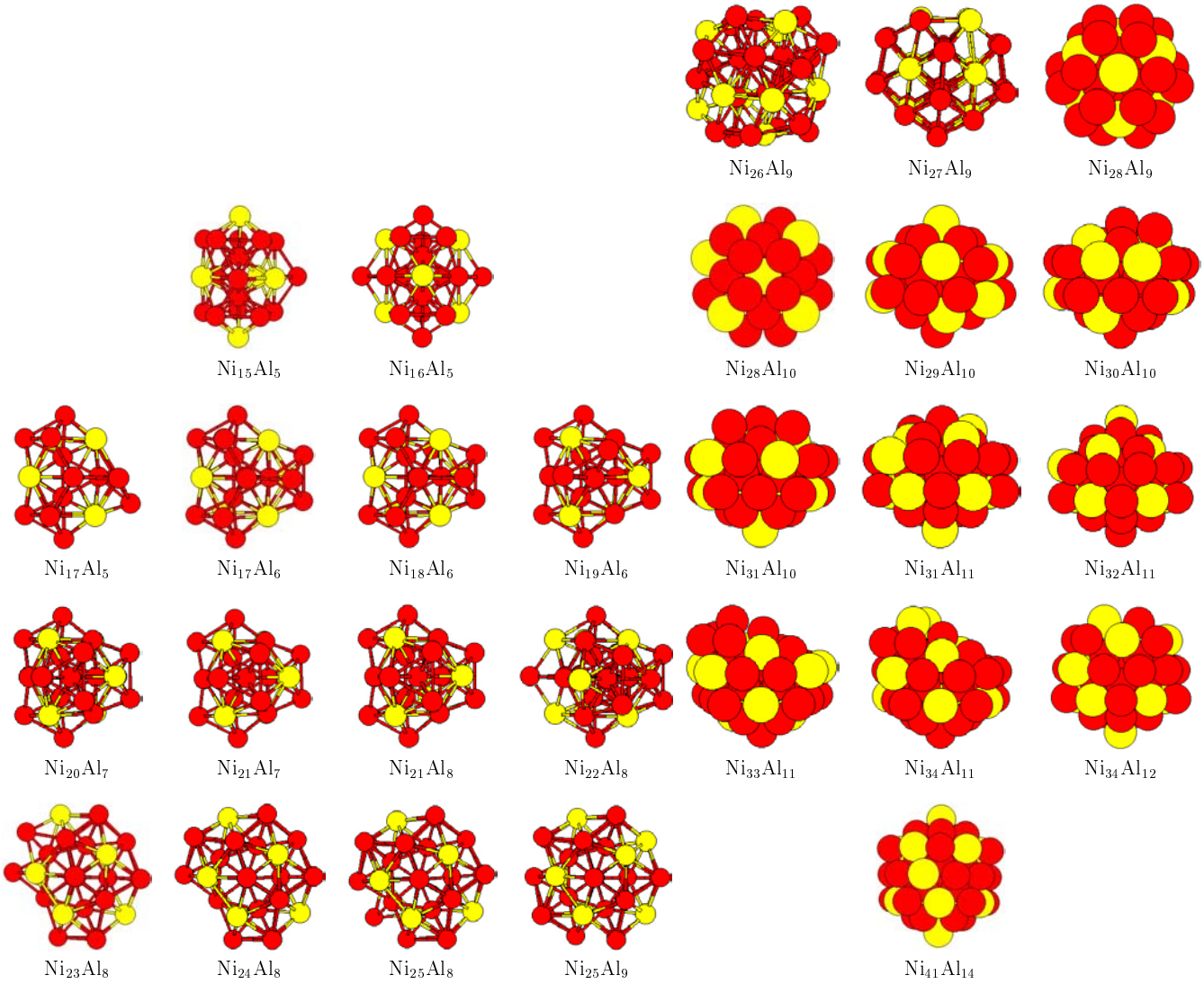

Fig. 8. GM found, using the GA, for 20–55-atom clusters with the approximate composition Ni_3Al. For simplicity, the larger clusters are represented by space-filling diagrams.

finding, it is likely that, in our application of the RSA, we may not have found all of the low lying homotops for $Ni_{10}Al_9$.

The global minima found, using the GA, for 20–55-atom clusters (with the approximate composition Ni_3Al) are shown in Figure 8. Three main features are evident in the growth patterns of these clusters. First, from 20–34 atoms (*i.e.* up to $Ni_{25}Al_9$), the GM consists of a DI core which is capped around the waist. The structure of $Ni_{26}Al_9$ is somewhat amorphous, though icosahedral packing motifs can again be seen. At this size there is an abrupt change to structures based on the truncated octahedron — which is complete for the 38-atom cluster $Ni_{28}Al_{10}$ — with local fcc packing, as in the bulk Ni_3Al structure. The truncated octahedral geometry has previously been found to be the GM for many 38-atom clusters (*e.g.* Ni_{38}, Cu_{38}, Ag_{38}, Au_{38} and $Cu_{19}Au_{19}$) bound by the Gupta many-body potential [40,50,51], as well as other many-body and pair potentials [38,44,55,56,73,74]. The structure of $Ni_{29}Al_{10}$ is a fragment of the 2-shell (55-atom) Mackay icosahedron. (The sudden switch from fcc-like to icosahedral-based was also observed by Wetzel and DePristo on going from Ni_{38} to Ni_{39} [55].) This structural motif is maintained for larger clusters, up as far as the largest cluster we have studied, $Ni_{41}Al_{14}$, which has the 2-shell centred-icosahedron geometry commonly found for 55-atom clusters [28,40,45,69,70]. Similar structures have been obtained for pure Ni clusters using the Gupta potential [50,51], though experimental studies by Parks, Riley and coworkers on N_2 adsorption on pure Ni clusters indicate that fcc structures may persist as far as Ni_{48}, with a transition to icosahedral structures occurring at Ni_{49} [60,62]. Finally, the closed geometric shell structures proposed for $Ni_{28}Al_{10}$ and Ni_{38} (truncated octahedra) and for $Ni_{41}Al_{14}$ and Ni_{55} (icosahedra) agree with the low electric dipole polarizabilities measured for corresponding pure Ni clusters by Knickelbein [76].

Considering homotop stability, it can be seen that the minority Al atoms are rarely situated next to each other, so the number of (stronger) Ni–Al contacts is maximized. This has also been observed by Rey *et al.* [19] and is consistent with Jellinek's findings [7,18]. Again interstitial Al atoms are rare, with the Al atoms preferring to lie on the surface of the cluster, which is again due to a combination of size and surface energy effects [18,19,22,71]. In their EAM studies, however, Rey *et al.* found that the most stable homotop of the 2-shell icosahedral $Ni_{54}Al$ cluster is that in which the Al atom occupies the inner-most 12-coordinate site, this being slightly more stable than a homotop where the Al atom lies in an edge site on the surface of the cluster [19]. This was attributed to the decreasing importance of size effects for larger clusters, so that the homotop stability is dominated by the maximization of Ni–Al interactions.

4 Conclusions

The detailed studies presented here have shown that the structures of the lowest energy isomers of Ni, Al and Ni-Al clusters are both size and composition dependent. Icosahedral structural motifs dominate, though there are regions of stability of other structures, such as those based on the truncated octahedron — with local fcc packing. Calculations on doped clusters have indicated that geometrical structures can be altered by doping a single Al or Ni atom into a pure cluster of the other metal. The GM structures of the pure metal and nanoalloy clusters have been compared with those obtained in previous studies and a good general agreement has been found in most cases, indicating that the various potentials employed in these studies are somewhat isomorphous, at least in the regions of conformation and composition space searched here. Discrepancies may arise due to differences in the exact functional forms of the potentials or to the different ways in which the potentials were parameterised. Comparisons with experimental results also show reasonable agreement.

In agreement with previous studies of nanoalloy clusters [7,18,19,22,28,40,71], we have found that homotop stability (*i.e.* whether there is segregation or ordering) is determined by a number of factors, which (depending on the cluster geometry, size and composition) may oppose or reinforce each other:

- maximization of the number of Ni–Al interactions (since the Ni–Al interaction is stronger than both the Ni–Ni and the Al–Al interactions) — this favours Ni-Al ordering;
- minimization of the cluster surface energy — this favours segregation, with the cluster surface becoming richer in the element (Al) which has the lower surface energy;
- minimization of bulk strain — this favours the location of the smaller atom (Ni) at the centre of icosahedral clusters.

It is worth remembering that, although the GA is more efficient than the RSA for finding global minima, especially in mixed-metal clusters [33,40], it is still possible (in particular for the larger clusters studied) that the lowest energy homotop may not have been found. It is very likely, however, that the correct lowest energy geometrical structure has been identified. Work is currently under way in order to improve the efficiency of the GA for finding optimum homotops for a given nuclearity, geometry and composition.

The authors wish to thank Professor Julius Jellinek and Dr. Alvaro Posada-Amarillas for helpful discussions and Mr Thomas Mortimer-Jones for help in preparing some of the figures. The authors are also grateful to a referee for helpful comments and suggestions. NTW and CR are grateful to the EPSRC for Ph.D. studentships.

References

1. R.L. Johnston, *Atomic and Molecular Clusters* (Taylor and Francis, London, 2002)
2. J. Jortner, Z. Phys. D **24**, 247 (1992)
3. R.L. Johnston, Phil. Trans. Roy. Soc. Lond. A **356**, 211 (1998)
4. W.B. Pearson, *The Crystal Chemistry and Physics of Metals and Alloys* (Wiley, New York, 1972)
5. S. Giorgio, H. Graoui, C. Chapan, C.R. Henry, in *Metal Clusters in Chemistry*, edited by P. Braunstein, L.A. Oro, P.R. Raithby (Wiley-VCH, Weinheim, 1999), Vol. 2, p. 1194
6. B. Pauwels, G. van Tendeloo, E. Zhurkin, M. Hou, G. Verschoren, L. Theil Kuhn, W. Bouwen, P. Lievens, Phys. Rev. B **63**, 165406 (2001)
7. J. Jellinek, E.B. Krissinel, in *Theory of Atomic and Molecular Clusters*, edited by J. Jellinek (Springer, Berlin, 1999), p. 277
8. A.V. Ruban, H.L. Skriver, J.K. Nørskov, Phys. Rev. B **59**, 15990 (1999)
9. A.M. Molenbroek, S. Haukka, B.S. Clausen, J. Phys. Chem. B **102**, 10680 (1998)
10. G. Schmid, in *Metal Clusters in Chemistry*, edited by P. Braunstein, L.A. Oro, P.R. Raithby (Wiley-VCH, Weinheim, 1999), Vol. 3, p. 1325
11. M.P. Andrews, S.C. O'Brien, J. Phys. Chem. **96**, 8233 (1992)
12. *Atomistic Simulation of materials: Beyond Pair Potentials*, edited by V. Vitek, D.J. Srolovitz (Plenum, New York, 1989)
13. A. Christensen, P. Stolze, J.K. Nørskov, J. Phys. Cond. Matt. **7**, 1047 (1995)
14. M.J. López, P.A. Marcos, J.A. Alonso, J. Chem. Phys. **104**, 1056 (1996)
15. J. Jellinek, E.B. Krissinel, Chem. Phys. Lett. **258**, 283 (1996)
16. E.B. Krissinel, J. Jellinek, Chem. Phys. Lett. **272**, 301 (1997)
17. E.B. Krissinel, J. Jellinek, Int. J. Quant. Chem. **62**, 185 (1997)
18. E.F. Rexer, J. Jellinek, E.B. Krissinel, E.K. Parks, S.J. Riley, J. Chem. Phys. **117**, 82 (2002)

19. C. Rey, J. García-Rodeja, L.J. Gallego, Phys. Rev. B **54**, 2942 (1996)
20. L. Zhu, A.E. DePristo, J. Chem. Phys. **102**, 5342 (1995)
21. L. Zhu, K.S. Liang, B. Zhang, J.S. Bradley, A.E. DePristo, J. Catal. **167**, 412 (1997)
22. J.M. Montejano-Carrizalez, M.P. Iñiguez, J.A. Alonso, Phys. Rev. B **49**, 16 649 (1994)
23. A. Fortunelli, A.M. Velasco, J. Mol. Struc. (Theochem) **487**, 251 (1999)
24. M. Calleja, C. Rey, M.M.G. Alemany, L.J. Gallego, P. Ordejón, D. Sánchez-Portal, E. Artacho, J.M. Soler, Phys. Rev. B **60**, 2020 (1999)
25. S. Bromley, G. Sankar, C.R.A. Catlow, T. Maschmeyer, B.F.G. Johnson, J.M. Thomas, Chem. Phys. Lett. **340**, 524 (2001)
26. F. Massicot, R. Schneider, Y. Fort, S. Illy-Cherrey, O. Tillement, Tetrahedron **56**, 4765 (2000)
27. F. Cleri, V. Rosato, Phys. Rev. B **48**, 22 (1993)
28. N.T. Wilson, R.L. Johnston, J. Mater. Chem. **12**, 2913 (2002)
29. B. Hartke, Chem. Phys. Lett. **258** 144 (1996)
30. J. Holland, *Adaptation in Natural and Artificial Systems* (University of Michigan Press, Ann Arbor, MI, 1975)
31. D.E. Goldberg, *Genetic Algorithms in Search, Optimization and Machine Learning* (Addison-Wesley, Reading, MA, 1989)
32. H.M. Cartwright, *Applications of Artificial Intelligence in Chemistry* (Oxford University Press, Oxford, 1993)
33. R.L. Johnston, C. Roberts, in *Soft Computing Approaches in Chemistry*, edited by H.M. Cartwright, L.M. Sztandera (Springer-Verlag, Heidelberg, 2003), pp. 161–204
34. O.J. Lanning, *Theoretical Study of Structures and Properties of Alloys*, M. Nat. Sci. 4th Year Project Report (University of Birmingham, 2001)
35. C. Kittel, *Introduction to Solid State Physics*, 6th edn. (John Wiley, New York, 1986)
36. L.D. Lloyd, R.L. Johnston, Chem. Phys. **236**, 107 (1998)
37. *NAG Fortran Library (Version 16)* (Numerical Algorithms Group, Oxford, 1993)
38. C. Roberts, R.L. Johnston, N.T. Wilson, Theor. Chem. Acc. **104**, 123 (2000)
39. D.M. Deaven, K.M. Ho, Phys. Rev. Lett. **75**, 288 (1995)
40. S. Darby, T.V. Mortimer-Jones, R.L. Johnston, C. Roberts, J. Chem. Phys. **116**, 1536 (2002)
41. R.A. Lordeiro, F.F. Guimarães, J.C. Belchior, R.L. Johnston, Int. J. Quant. Chem. (in press)
42. C. Massen, T.V. Mortimer-Jones, R.L. Johnston, J. Chem. Soc., Dalton Trans. 4375 (2002)
43. R. Ahlrichs, S.D. Elliott, Phys. Chem. Chem. Phys. **1**, 13 (1999)
44. J.P.K. Doye, D.J. Wales, New J. Chem. **22**, 733 (1998)
45. J.P.K. Doye, D.J. Wales, J. Phys. B **29**, 4859 (1996)
46. L.D. Lloyd, R.L. Johnston, J. Chem. Soc., Dalton Trans. 307 (2000)
47. L.D. Lloyd, R.L. Johnston, C. Roberts, T.V. Mortimer-Jones, Chem. Phys. Chem. **3**, 408 (2002)
48. J. Jellinek, in *Metal–Ligand Interactions*, edited by N. Russo, D.R. Salahub (Kluwer, Dordrecht, 1996), p. 325
49. M. Böyükata, Z.B. Güvenç, S. Özçelik, P. Durmus, J. Jellinek, Int. J. Quant. Chem. **84**, 208 (2001)
50. K. Michaelian, N. Rendón, I.L. Garzón, Phys. Rev. B **60**, 2000 (1999)
51. A. Posada Amarillas, M.F. Ortíz, C. Roberts, T.V. Mortimer-Jones, R.L. Johnston, manuscript in preparation
52. S.K. Nayak, S.N. Khanna, B.K. Rao, P. Jena, J. Phys. Chem. A **101**, 1072 (1997)
53. Y. Xiang, D.Y. Sun, X.G. Gong, J. Phys. Chem. A **104**, 2746 (2000)
54. M.S. Stave, A.E. DePristo, J. Chem. Phys. **97**, 3386 (1992)
55. T.L. Wetzel, A.E. DePristo, J. Chem. Phys. **105**, 572 (1996)
56. N.N. Lathiotakis, A.N. Andriotis, M. Menon, J. Connolly, J. Chem. Phys. **104**, 992 (1996)
57. E.K. Parks, L. Zhu, J. Ho, S.J. Riley, J. Chem. Phys. **100**, 7206 (1994)
58. E.K. Parks, L. Zhu, J. Ho, S.J. Riley, J. Chem. Phys. **102**, 7377 (1995)
59. E.K. Parks, G.C. Nieman, K.P. Kerns, S.J. Riley, J. Chem. Phys. **107**, 1861 (1997)
60. E.K. Parks, G.C. Nieman, K.P. Kerns, S.J. Riley, J. Chem. Phys. **108**, 3731 (1998)
61. E.K. Parks, K.P. Kerns, S.J. Riley, Chem. Phys. **262**, 151 (2000)
62. E.K. Parks, K.P. Kerns, S.J. Riley, J. Chem. Phys. **114**, 2228 (2001)
63. E.K. Parks, E.F. Rexer, S.J. Riley, J. Chem. Phys. **117**, 95 (2002)
64. J.P.K. Doye, D.J. Wales, R.S. Berry, J. Chem. Phys. **103**, 4234 (1995)
65. F.C. Frank, J.S. Kasper, Acta. Cryst. **11**, 184 (1958)
66. M.S. Bailey, N.T. Wilson, R.L. Johnston, manuscript in preparation
67. A.R. Miedema, Z. Metallkde. **69**, 287 (1978)
68. W.R. Tyson, W.A. Miller, Surf. Sci. **62**, 267 (1977)
69. J. Xie, J.A. Northby, D.L. Freeman, J.D. Doll, J. Chem. Phys. **91**, 612 (1989)
70. J.E. Hearn, R.L. Johnston, J. Chem. Phys. **107**, 4674 (1997)
71. A.M. Schoeb, T.J. Raeker, L.Q. Yang, X. Wu, T.S. King, A.E. DePristo, Surf. Sci. **278**, L125 (1992)
72. R.R. Hultgren, P.D. Desai, D.T. Hawkins, M. Gleiser, K.K. Kelley, *Selected Values of the Thermodynamic Propereties of Binary Alloys* (American Soc. Metals, Ohio, 1973)
73. J.P.K. Doye, D.J. Wales, J. Chem. Soc., Faraday Trans. **93**, 4233 (1997)
74. N.T. Wilson, H. Cox, R.L. Johnston, manuscript in preparation
75. S.K. Lai, P.J. Hsu, K.L. Wu, W.K. Liu, M. Iwamatsu, J. Chem. Phys. **117**, 10715 (2002)
76. M.B. Knickelbein, J. Chem. Phys. **115**, 5957 (2001)